ELSEVIER

NeuroImage

www.elsevier.com/locate/ynimg
NeuroImage 42 (2008) 207–217

A method for spatiotemporal mapping of event-related modulation of cortical rhythmic activity

H. Laaksonen,* J. Kujala, and R. Salmelin

Brain Research Unit, Low Temperature Laboratory, Helsinki University of Technology, Espoo, Finland

Received 17 January 2008; revised 3 April 2008; accepted 5 April 2008
Available online 22 April 2008

Cortical rhythmic activity can be systematically modulated by stimuli or tasks and may thus provide relevant information about brain function. Meaningful use of those phenomena requires characterization of both locations and time courses of event-related suppressions and increases of oscillatory activity. However, localization of the neural sources of cortical rhythms during intervals of very low levels of activity, and within short time intervals, is not a trivial matter. Hence, event-related modulation of rhythmic activity has typically been described at the level of magnetoencephalography (MEG) sensors or electroencephalography (EEG) electrodes, without reaching into the brain. Here, we introduce erDICS, an event-related version of Dynamic Imaging of Coherent Sources that allows spatial mapping of the level of oscillatory activity in the brain as a function of time, with respect to stimulus or task timing. By utilizing a time-resolved frequency-domain beamformer, erDICS yields the spatial distribution of both power suppressions and power increases. Permutation tests further reveal areas and time windows in which the modulations of oscillatory power are statistically significant, in individual subjects. We demonstrate the usability of erDICS on simulated and real MEG data. From the erDICS maps we identify areas showing salient event-related changes of rhythmic activity, represent them with equivalent current dipoles and calculate their contribution to the measured signal. Comparison of this multidipole model with the original signal yields a quantitative measure of goodness for the identified source areas and the analysis approach in general.

Introduction

Magnetoencephalography (MEG) and electroencephalography (EEG) provide a continuous real-time measure of neural activity. Activation sequences associated with performing specific tasks or processing different stimuli are typically studied by averaging the measured signal across repeated trials, aligned to stimulus or task onset, and by focusing on the so-called evoked responses that emerge from the noise. These "noise" signals, however, may also contain potentially interesting information. The cerebrum exhibits rhythmic activity the modulation of which is, unlike the evoked responses, often not phase-locked to stimulus or task timing and is, therefore, eliminated when the data is averaged across trials. This event-related modulation of rhythmic activity may well provide information about neural activity that is complementary to that obtained with evoked responses (Salmelin et al., 2000). The best known modulations of rhythmic activity are movement-related suppressions and enhancements (Chatrian et al., 1959; Pfurtscheller, 1992; Pfurtscheller and Aranibar, 1979; Pfurtscheller and Lopes da Silva, 1999; Salmelin and Hari, 1994; Salmelin et al., 1995), but task-related modulations have also been found during, e.g., visual search and working memory tasks (Jensen et al., 2002; Tallon-Baudry et al., 1997). In particular, increased synchrony of rhythmic firing within a neural population, which may show as an overall higher level of oscillatory activity in MEG/EEG signals, has been suggested to play a role in the binding problem, i.e., merging of different types of information (e.g., color, shape, motion) into a unified percept (Singer, 1999). In addition, it has been suggested that the spatial distribution of brain areas in which the level of rhythmic activity is affected by task corresponds to the spatial pattern of activation obtained with functional magnetic resonance imaging (fMRI) (Singh et al., 2002), and that the correspondence between electrophysiological and hemodynamic measures might be particularly pronounced for the gamma band (40–100 Hz) (Brookes et al., 2005; Foucher et al., 2003; Niessing et al., 2005). Rhythmic activity and synchrony at the neuronal population level are not directly accessible with hemodynamic imaging methods (fMRI; positron emission tomography, PET). Therefore, although accurate localization is not the main strength of neurophysiological methods, it is crucial to develop analysis approaches for neurophysiological data that allow reliable quantitative characterization of task-related modulations of rhythmic activity in both space and time. Such quantification is particularly feasible for MEG which lends itself more readily for spatial mapping than EEG.

* Corresponding author. Brain Research Unit, Low Temperature Laboratory, P.O. Box 5100, FIN — 02015 TKK, Finland. Fax: +358 9 451 3508.
E-mail address: hannu@neuro.hut.fi (H. Laaksonen).
Available online on ScienceDirect (www.sciencedirect.com).

1053-8119/$ - see front matter © 2008 Elsevier Inc. All rights reserved.
doi:10.1016/j.neuroimage.2008.04.175

In EEG/MEG the forward problem, i.e., calculation of electromagnetic field when the source currents are known, has a unique solution. The inverse, however, i.e., determining the distribution of source currents within the brain from the electromagnetic fields measured outside of the head cannot be performed unequivocally as, theoretically, one may construct an infinite number of source current configurations that would generate an identical electromagnetic field outside of the head. In practice, physical and physiological realities set reasonable constraints to facilitate this analysis (Hämäläinen et al., 1993; Lounasmaa et al., 1996). A frequently used solution is to define the brain as a spherical conductor and to model centers of active brain areas with point-like sources, referred to as equivalent current dipoles (ECDs). An ECD represents the center of an active cortical patch and the mean orientation and strength of electric current therein (Hämäläinen et al., 1993).

ECD analysis has been used to localize the sources of rhythmic activity, by finding best-fitting ECDs every few milliseconds over extended intervals of strong oscillatory activity (Liljeström et al., 2005). While ECD analysis reliably localizes, e.g., movement-related enhancement of motor cortex 20-Hz activity (Salmelin and Hari, 1994; Salmelin and Sams, 2002) it is perhaps not best suited for analysis of rhythmic activity in general. The approach requires a considerable amount of manual work and an experienced user, e.g., when selecting the appropriate subsets of sensors for focusing on the different source areas (Liljeström et al., 2005). Furthermore, sources can only be localized for high levels of rhythmic activity whereas areas showing suppression of rhythmic activity cannot be identified directly because of the poor signal-to-noise ratio; it may be possible to deduce such areas indirectly if they also show high levels of oscillatory activity at another point in time.

Analysis methods for simultaneous localization of sources of rhythmic activity based on beamformers (Van Veen and Buckley, 1988) have been developed recently (Cheyne et al., 2000; Gross et al., 2001; Robinson and Vrba, 1997). These approaches employ a spatial filter to reach from sensor-level signals to activity maps estimated throughout the brain volume. The main drawback of beamformer techniques is that, theoretically, they cannot identify source areas with perfectly correlated time courses of activation. In practice, however, even highly correlated sources can be determined in realistic noisy MEG data (Sekihara et al., 2004; Van Veen et al., 1997). In this work we focus on Dynamic Imaging of Coherent Sources (DICS), a method originally developed for mapping coherence and power of oscillatory activity in continuous tasks (Gross et al., 2001). DICS is a linearly constrained minimum variance beamformer (Van Veen et al., 1997), which aims to maximize the signal from a given location while minimizing the interference from other source areas. It uses cross-spectral density (CSD) matrix to represent the oscillatory components and their linear dependencies, and the spatial filter is defined separately for each frequency range (Gross et al., 2001).

A related method called Synthetic Aperture Magnetometry (SAM) (Robinson and Vrba, 1997) has recently been used for studying modulation of rhythmic activity (Furlong et al., 2004; Gaetz and Cheyne, 2006; Pammer et al., 2004; Singh et al., 2002). Similar to DICS, SAM is an adaptive beamformer technique which associates each point in the brain with a set of weights for MEG sensors. The main difference between the methods is that in SAM the analysis is performed in the time domain and the sensor-level data is represented by the covariance matrix. The MEG data is passed through the spatial filters defined at grid points covering the brain and, thereafter, filtered to the desired frequency band.

Oscillatory brain activity has also been investigated with methods based on minimum current estimates (Jensen and Vanni, 2002) and minimum norm estimates (Lin et al., 2004). Both of these methods belong to the class of distributed source models, i.e., they simultaneously estimate multiple sources. In order to access rhythmic activity, the estimates are based on Fourier or wavelet transformed MEG signals. Anatomical constraints for the sources, e.g., based on fMRI experiments can be added to the model (Dale et al., 2000; Lin et al., 2004).

Most of these methods have been applied to experiments that use a so-called 'block design' in which one task/stimulus type is presented in a row, a setup commonly employed in fMRI studies. MEG and EEG experiments more typically rely on 'event-related' designs in which tasks/stimulus types vary randomly. SAM has recently been applied to such setups as well (Cheyne et al., 2006; McNab et al., 2007; Pammer et al., 2006, 2004).

Here, we present the event-related DICS (erDICS) method that allows study of modulations of oscillatory activity as a function of time with respect to triggers. These triggers can be, e.g., onsets of external stimuli or self-paced tasks. A wavelet-based filter bank approach is used to estimate the frequency distribution within short time intervals, which is then employed in calculation of time-dependent CSD. The wavelet approach offers a better compromise between time and frequency resolution than a typical short-term Fourier transform. Prior to this work, DICS was best suited for investigations of oscillatory activity in continuous tasks. With the modifications presented here, the method can be more flexibly used to study event-related modulations of rhythmic activity. By comparing different time instances, besides studying increases in rhythmic activity it is also possible to directly assess decreases, i.e., suppressions. Furthermore, the time-dependent CSD lends itself naturally to mapping of event-related coherence as well, although the present study focuses on the time-resolved localization of oscillatory power.

As power maps are influenced by the overall levels of neural activity and noise, they may provide a partly erroneous view of brain function. Here, in order to enhance the reliability of the mapping of rhythmic activity statistical representations are generated by utilizing maximum-statistics permutation testing (Holmes et al., 1996; Maris and Oostenveld, 2007; Nichols and Holmes, 2002; Pantazis et al., 2005). Considering the substantial interindividual variation of the spatial and frequency distribution of rhythmic activity across humans (Steriade et al., 1990) we will focus on individual-level statistical tests since they are likely to provide a clearer picture of rhythmic activity than direct group-level evaluation. A permutation test requires two distributions of values for comparison (for instance, power levels from "baseline" and "active" time segments). We consider two alternative procedures for performing the statistical test. In one approach, power maps are computed separately for each single trial, which is a straightforward way of acquiring the sample distributions. However, this method suffers from a poor signal-to-noise ratio (SNR) which might render the single-trial power maps useless. In the other approach, we use the spatial filter defined in erDICS with the CSD averaged over trials to estimate the time course of activity at each voxel in the brain and to gather the needed distributions from these source-level time series. As a potential limitation, this technique makes the assumption that the source locations and main directions of current flow in a voxel remain essentially unchanged over trials.

For any neuroimaging analysis approach it is essential to verify that the identified brain areas and the modulation of activity therein account for the original measured signals. From the erDICS maps

we identify areas showing salient event-related changes in the level of rhythmic activity, represent them with ECDs, estimate the time course of activity in those areas and calculate their contribution to the measured signal. Comparison of this model with the original measured event-related modulation of cortical rhythms yields a quantitative measure of goodness for the source model and the analysis approach in general. Here, we demonstrate the usability of erDICS with the help of simulations and two real data sets, one recorded during self-paced finger movements and the other during a reading task.

Methods

Analysis steps

The first step of the erDICS analysis is to define the frequency range of interest (Fig. 1, box A). The initial evaluation was done by inspecting the frequency spectra of the MEG sensor signals, calculated over the entire data set. More detailed estimation included time-frequency representation (TFR, Tallon-Baudry et al., 1997) plots that display frequency content of the signal as a function of time, aligned to trigger onsets and averaged across trials, and temporal spectral evolution curves (TSE, Salmelin and Hari, 1994) that depict the mean amplitude of rhythmic activity in a selected frequency band as a function of time, with respect to trigger onset. These methods help to identify frequency ranges and time windows in which there are systematic stimulus/task-related decreases and increases of rhythmic activity. These frequency and time ranges are employed in the following steps of the analysis procedure. All the computations can be done for all frequencies; here, we evaluate the CSD only for the selected frequencies in order to save time, computing power and memory space. Furthermore, we can use frequency bands specific for the data, which improves the SNR of the CSD estimate.

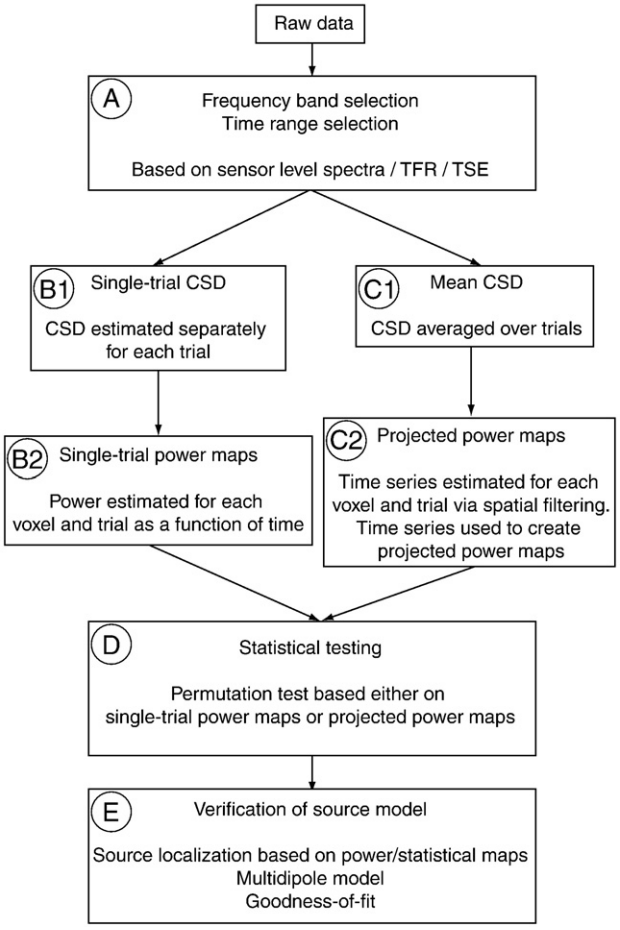

Fig. 1. Flow chart of the analysis procedure. Box A: The frequency band of interest is selected first, prior to use of erDICS, with the help of sensor-level spectra, time-frequency representations (TFR) and temporal spectral evolution (TSE) curves. Boxes B, C: Two alternative ways of estimating power maps, using the cross-spectral density matrix (CSD). Box D: Statistical testing of power maps. Steps B–D are done in erDICS mainly automatically, without a need for user interaction. Box E: Verification of the source model is done in user-controlled iterative steps. Source areas are identified, a source model is constructed and the resulting model is compared with the measured data.

In the second phase (Fig. 1, boxes B1 and C1) we move from sensor level to the level of the brain with the help of the cross-spectral density matrix (Gross et al., 2001). The CSD is obtained as the product of Fourier transformed signals as

$$\mathbf{C}_{ij}(f) = \mathbf{X}_i(f)^*\mathbf{X}_i(f), \tag{1}$$

where $\mathbf{C}$ represents the CSD, $\mathbf{X}$ is the Fourier transform of the originally recorded MEG sensor signal, f is the frequency and indices i and j run over all sensors.

In order to incorporate time information (erDICS) we estimated the CSD from short time segments of the measured data by applying a filter bank composed of complex Morlet wavelets. The Morlet wavelet M is basically a sinusoid modulated with a Gaussian envelope function, defined as (modified from Tallon-Baudry et al., 1997):

$$M(t, f_c, \sigma_t) = Se^{-t^2/2\sigma_t^2}e^{j2\pi f_c t}, \tag{2}$$

where t is time, f_c is the center frequency of the wavelet and σ_t its standard deviation in the time domain. The scaling parameter S is defined as $S = (\sigma_t\sqrt{\pi})^{-1/2}$. The standard deviation of the wavelet profile in time (σ_t) and frequency (σ_f) are linked via the equation

$$\sigma_f = 1/(2\pi\sigma_t). \tag{3}$$

The ratio $w = f_c / \sigma_f$ controls the trade-off between time and frequency resolution and is referred to as the wavelet "width" (Tallon-Baudry et al., 1997). Using these definitions the full width at half maximum (FWHM) of Morlet wavelets in time (w_t) and frequency domain (w_f) for a given wavelet width and center frequency are defined as

$$\begin{aligned} w_t &= \sqrt{2^*\ln 2}/\pi^* w/f_c, \\ w_f &= \sqrt{2^*\ln 2}^* f_c/w. \end{aligned} \tag{4}$$

Here we used the definition of FWHM for Gaussian distribution. The temporal resolution is degraded with larger wavelet width and improves at higher frequencies. The reverse applies for frequency resolution. In this work we used wavelet width of 10, yielding $w_f = 0.23548 * f_c$ and $w_t = 3.748 / f_c$.

By substituting the Fourier transformed signal in Eq. (1) with signal filtered according to Eq. (2), a time and frequency-dependent CSD ($C_{ij} = C_{ij}(f,t)$) is acquired. It can be estimated separately for each trial ("single-trial CSD") or averaged across all trials ("mean CSD").

In the next step (Fig. 1, boxes B2 and C2), the analysis proceeds from MEG sensor-level signals to cortical activity. DICS/erDICS uses a beamformer that is created by combining the CSD matrix with the geometry of the subject's brain, either in the form of a spherical model or a realistic boundary-element model (BEM, Hämäläinen and Sarvas, 1989). The choice of geometry defines the forward problem solutions, or lead fields, and is a significant parameter in beamformer analysis. Here, the spherical model was used because of its simplicity and robustness. The power distribution is estimated in a grid covering the brain volume, and is done with a linear transformation referred to as a spatial filter. The spatial filter is specified in form of a transformation matrix **A** (Gross et al., 2001):

$$\mathbf{A}(\mathbf{r},f,t) = \left(\mathbf{L}^T(\mathbf{r})\mathbf{C}_\mathbf{r}^{-1}(f,t)\mathbf{L}(\mathbf{r})\right)^{-1}\mathbf{L}^T(\mathbf{r})\mathbf{C}_\mathbf{r}^{-1}(f,t), \quad (5)$$

where $\mathbf{L}(\mathbf{r})$ is the solution to the forward problem at location $\mathbf{r}$, and $\mathbf{C}_\mathbf{r} = \mathbf{C} + \alpha\mathbf{I}$, with $\mathbf{C}$ as the CSD matrix and α the regularization parameter. The power estimate at a given location is

$$\mathbf{P}(\mathbf{r},f,t) = \mathbf{A}(\mathbf{r},f,t)\mathbf{C}(f,t)\mathbf{A}^T(\mathbf{r},f,t). \quad (6)$$

Beamforming with time-varying CSDs allows comparison of spectral power at different time intervals, for example, between an "active" post-stimulus interval and a pre-stimulus "baseline" interval (cf. Fig. 1, box A) and, thus, localization of brain areas that display relative increases and decreases in the level of rhythmic activity. We evaluated the power maps in two alternative ways: (i) single-trial CSDs (Fig. 1, box B1) were used to estimate power maps separately for each trial as defined in Eq. (6). These single-trial power maps (Fig. 1, box B2) were then subjected to further analysis (averaging across trials, statistical testing). (ii) The mean CSD (Fig. 1, box C1), averaged across trials, was used to create a spatial filter that was applied to the raw data to extract the time course of activity at each voxel. The raw data was further band-pass filtered and the instantaneous amplitudes were estimated with Hilbert transform. Projected power maps (Fig. 1, box C2) refer to estimation of power (i.e., square of amplitude) maps in each trial via the voxel time courses.

Statistical testing

For evaluating statistical significance of the observed power changes the trial-to-trial distribution of activation is needed per voxel. We collected those values in two ways, by using single-trial CSDs (and usual single-trial power maps) and mean CSD (and time series from projected power maps), as described above. The two approaches were tested on the same data set (Fig. 1, box D).

In order to estimate statistical difference between two time periods (here, "active" and "baseline"), we performed a random permutation test on the trial-to-trial power levels in each voxel. Random permutation test belongs to the class of nonparametric tests and makes minimal assumptions about the data, mainly that exchangeability of labels is valid (Holmes et al., 1996). Here, we can state that under the null hypothesis ("no difference") the labels "active" and "baseline" are interchangeable.

The voxel-based random permutation test was implemented as follows: first, a statistic comparing two distributions (i.e., trial-to-trial power levels in the "active" and "baseline" intervals) was calculated per voxel ("original" statistic). Any statistic can be used, and we used a common Student's *t*-test for this purpose. Second, the samples in the two distributions were permuted randomly and a new *t*-value was acquired. This step was repeated 5000 times and all the *t*-values were recorded into a new distribution ("test distribution"). The *p*-value for each voxel was estimated by checking how much of the test distribution was below (or above) the original *t*-value.

To decrease the amount of Type I errors (false positives) due to multiple comparisons, a maximum-statistics approach was applied. To this end, we collected the maximum and minimum *t*-values from the test distributions in each voxel ("maximum" and "minimum" distributions). These values defined new test distributions across voxels, and the final *p*-values were estimated by comparing the original *t*-values in each voxel to the maximum/minimum distributions across voxels in the same manner as in the regular permutation test (separate one-tailed tests). By looking at the distributions based on maximum or minimum *t*-values we can distinguish between increases and decreases of rhythmic activity.

Verification of the source model

In the final stage (Fig. 1, box E) a quantitative estimate was obtained on whether modulation of rhythmic activity in the identified brain areas indeed accounted for the stimulus/task-related modulation originally measured by the MEG sensors. Here, procedures that are typically used in the analysis of time-locked evoked responses were adopted as follows: brain areas showing event-related increase/suppression of rhythmic activity, i.e., local maxima/minima of erDICS maps, were modeled as ECDs. The orientations of the ECDs were acquired by first estimating source orientations at the investigated time point. As these estimates are influenced by background brain activity and noise, the orientations were calculated also in the baseline interval. The final source orientations were then computed by subtracting the baseline orientation from the orientation at the investigated time point (with both orientations weighted by the corresponding power estimates), thus obtaining an orientation that is assumed to more specifically reflect the activity of interest during task or stimulus processing. Alternatively, one could use, e.g., mean of the orientations in the baseline and target intervals or orientation during the time period of maximum power for all time points.

The quality of the resulting multi-dipole model was evaluated by calculating the sensor-level TSE curves that activity in those source areas would generate, and by comparing those curves with the original TSE of the measured MEG signals. A goodness-of-fit value *g* was calculated, which gives a quantitative measure on how well the model fits the data:

$$g^2 = \frac{1}{T}\sum_t\left(1 - \frac{\sum_i (b_i(t) - b_i'(t))^2}{\sum_i b_i(t)^2}\right), \quad (7)$$

where $b_i(t)$ represents the measured signal and $b_i'(t)$ the signal generated by the constructed dipole model for sensor i at time *t*. In this work the *g*-value was averaged over all sensors and the entire epoch length (*T* is the total number of time samples). The final set of ECDs was acquired by iteratively adding and removing sources based on the projected power and statistical maps until a satisfactory model with a high goodness-of-fit value was reached.

Measured MEG data

The real MEG data sets were recorded with a Neuromag Vectorview™ 306-channel whole-head neuromagnetometer (Elekta Neuromag Ltd, Helsinki, Finland). The system contains 102 triple sensor

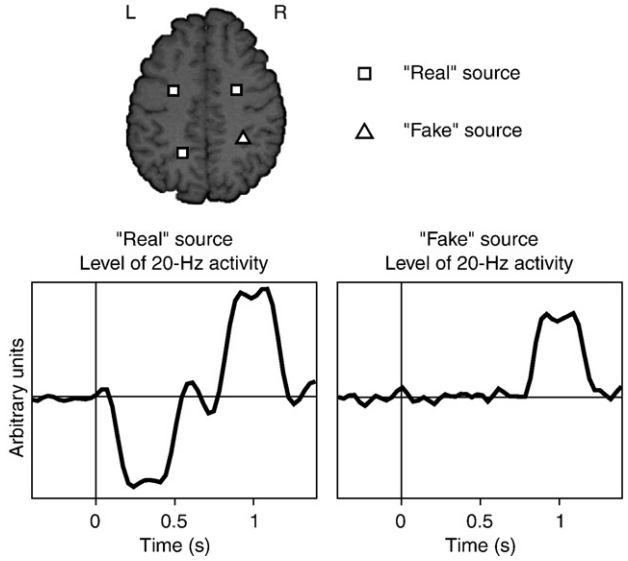

Fig. 2. Simulated sources. Three "real" sources (white squares) were placed in the left and right hand motor cortex and in the left posterior parietal cortex (above). These sources showed initial suppression of 20-Hz activity, followed by a rebound, as illustrated by the mean TSE curve across simulated trials (below, left). A "fake" source was also included (white triangle; top). It displayed an artefactual strong rebound of rhythmic activity in 5% of the trials that was evident in the average TSE curve (below, right).

elements composed of two orthogonal planar gradiometers and one magnetometer. The planar gradiometers detect the maximum signal directly above an active cortical area; in this study, the analysis was performed using the gradiometers. The data was band-passed to 0.03–200 Hz and sampled at 600 Hz. In all erDICS analyses the brain was divided into grid points with a grid size of 10 mm. In the first data set, the subjects were instructed to lift the index finger every 5 s (Saarinen et al., 2006). Left and right index lifts were performed in separate runs. In the second data set, the subjects were instructed to silently read written words that were presented every 3 s (Wydell et al., 2003).

Simulated MEG data

For initial validation of erDICS, a simple simulated MEG data set was generated with the same sampling frequency as for the real MEG data, using the 204 gradiometers. The time series of the simulated dipolar sources were forward-modeled to each sensor and, thereafter, white noise was linearly added. The simulation contained three "real" sources (Fig. 2). Oscillatory activity was modeled with sine waves. The instantaneous frequencies of the signals were modulated between 18.5–21.5 Hz (at different time points) in order to decrease coherence between sources. An additional fourth source represented

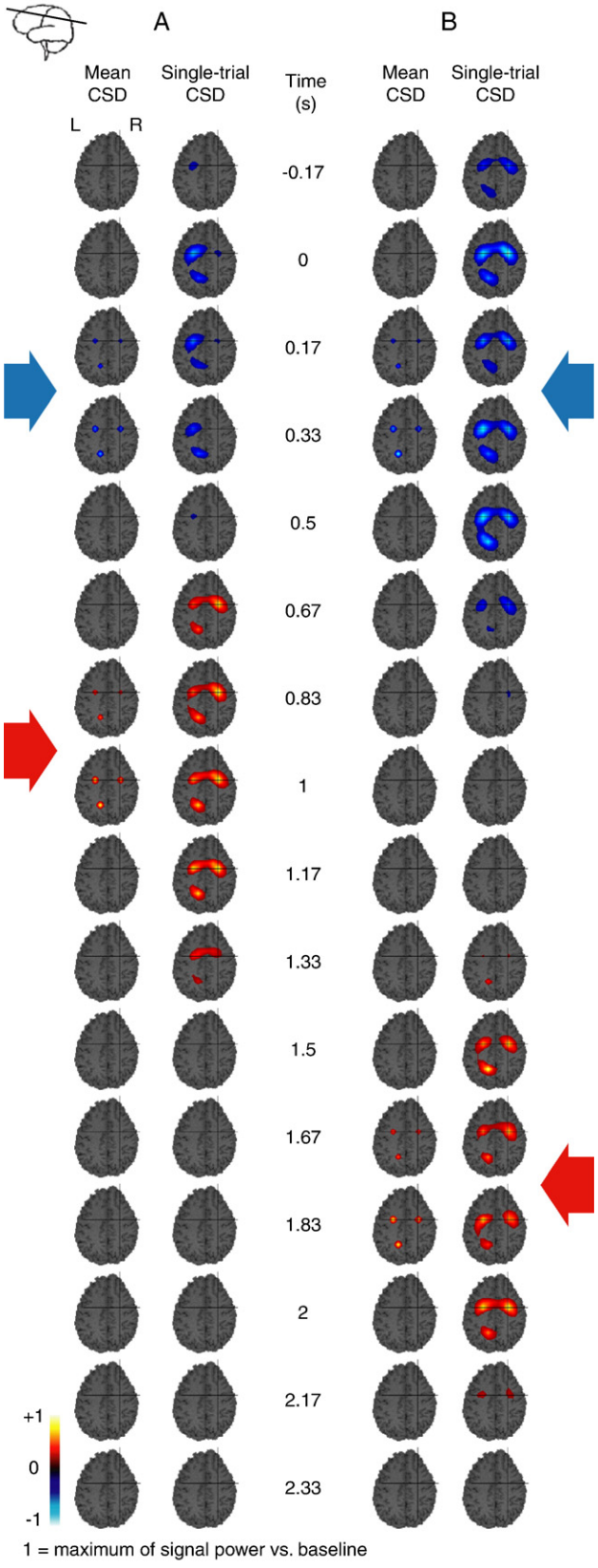

Fig. 3. Comparison between "mean CSD" projected power maps and "single-trial CSD" power maps. Blue and red arrows indicate the actual timing of simulated suppression and rebound, respectively. The delay between end of suppression and beginning of rebound was 0.3 s in case A and 1.2 s in case B. Color indicates decrease (blue) and increase (red/yellow) of rhythmic activity. In the case of "single-trial CSD" the activity spread out in time and, therefore, the contributions of suppression and rebound overlapped when they occurred close in time. The baseline interval was set at −100 to −67 ms. (For interpretation of the references to color in this figure legend, the reader is referred to the web version of this article.)

a "fake" source that produced activity in strong bursts (20 times stronger than in real sources) in 1/20 of the trials, coinciding with the increased 20-Hz activity in the real sources. The SNR was defined as the ratio between Frobenius norms of signal and noise.

Results

Simulations

Fig. 3 illustrates the projected power maps for "mean CSD" and estimated power maps for "single-trial CSD" approaches with the simulated data, at SNR of 1/5. When the end of the suppression and the beginning of the rebound were separated by 0.3 s, the "mean CSD" yielded the correct locations of suppressions and increases of rhythmic activity at the correct times (Fig. 3A). However, in the "single-trial CSD" the time windows of modulation effects were spread out, mainly due to the poor SNR of single-trial CSD. The limited time resolution of the wavelet approach further complicates the matter and causes temporally close suppressions and rebounds to overlap, which diminishes both effects. The resulting blurring of power maps prevented reliable estimation of the exact timing of the modulation of suppression and rebound. When the time delay between the subsequent modulations was increased to 1.2 s (Fig. 3B), the "single-trial CSD" maps became more accurate in time but remained spatially more spread out than in the "mean CSD". Accordingly, in the following, we use only the "mean CSD" approach for statistical testing.

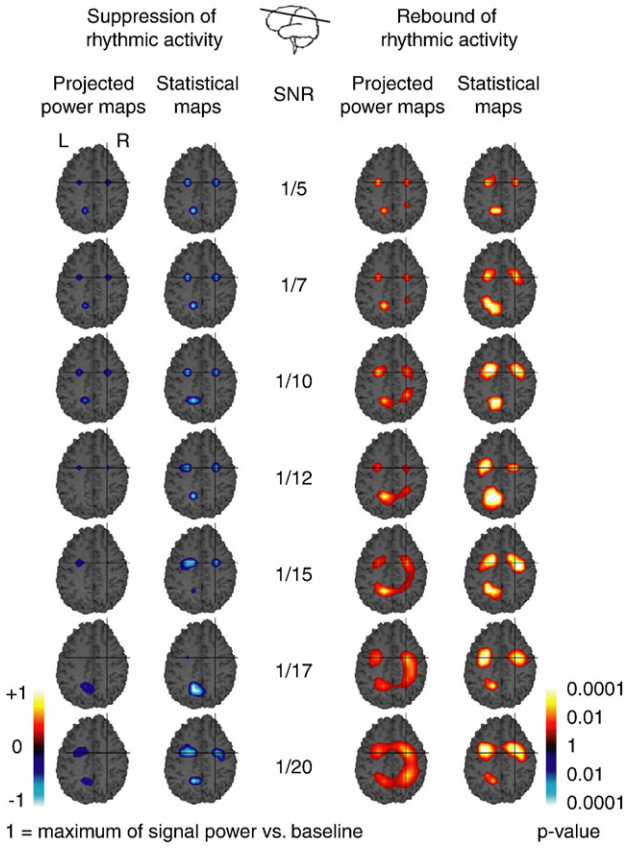

Fig. 4. Effect of SNR on the projected power and statistical maps of simulated data. The maps were plotted at two time points, one during the suppression phase (0.3 s) and the other during the rebound phase (1 s). The baseline interval was set at −100 to −67 ms. In the projected power maps, the maxima for suppression and rebound were at the correct location for SNRs down to 1/15; at lower SNRs, most of the sources were still localized to the correct location. Suppression was not fully detected below SNR 1/15. The statistical maps indicated that the maxima representing the "real" sources in the projected power maps represented areas with significant changes in rhythmic activity. The "fake" source was evident in the power maps but was eliminated in the statistical maps.

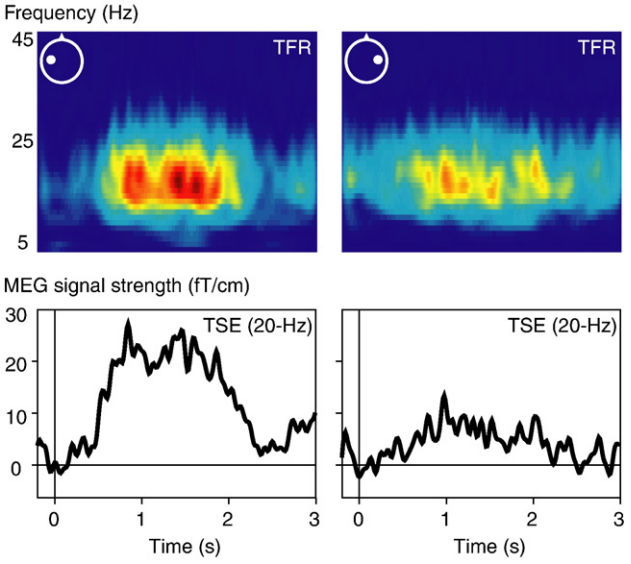

Fig. 5. Selection of frequency ranges and time windows in the finger lifting task. TFR plots and TSE curves during right index finger movement for selected single sensors over the left and right sensorimotor cortex (see schematic heads in the TFR plots). Rhythmic activity in the 20-Hz band (14–27 Hz) was enhanced strongly over the left hemisphere, and somewhat less markedly over the right hemisphere, at 0.4 to 2.2 s after movement onset.

The effect of noise on accuracy and sensitivity of erDICS was investigated by starting from typical SNR observed in MEG measurements and then decreasing the SNR to observe how the method handles very noisy situations (Fig. 4). All the simulated cortical sources were identified down to SNR of 1/15, both in the power maps and in the statistical maps, and they displayed the correct time behavior. As the noise level was increased, the maxima/minima became spatially more spread out. At very low SNR (1/20), the suppression was no longer detected, as noise started to dominate the signal, but the rebound was still evident. In addition to the three "real" sources, the "fake" source was evident in the power maps but it was eliminated in the statistical maps.

The localization accuracy of the simulated power and statistical maps was tested by performing the calculations with grid sizes decreasing from 10 mm to 1 mm, at 1-mm steps. At an SNR of 1/5, for all tested grid sizes, each simulated source was found at the correct grid point (i.e., the localization error was less than half the voxel size). The maxima were found at the correct locations down to SNR = 1/15, and at SNRs 1/17 and 1/20 the maxima were either at the correct location or fell on the immediately neighboring grid point.

Index finger movement task

Fig. 5 displays the TFR plot and TSE curves on one sensor over the left and one sensor over the right Rolandic area when the

subject lifted the right index finger. The frequency range used in the TSE was 14–27 Hz, which showed high level of activity in the TFR. This frequency range is typically modulated in motor tasks (Pfurtscheller and Lopes da Silva, 1999; Salmelin and Hari, 1994; Salmelin and Sams, 2002). There was a salient rebound of rhythmic activity above the pre-movement level starting at about 0.4 s after movement onset and continuing until about 2.2 s.

The erDICS projected power maps (Fig. 6) revealed a spatio-temporal pattern that was in good agreement with the TSE curves. The level of 20-Hz activity in the primary motor cortex was increased starting at about 0.5 s. In this subject, the effect was bilateral for the left index finger movement and more lateralized for the right index finger movement. The statistical maps (Fig. 6) confirmed that the enhanced rhythmic activity evident in the projected power maps was significantly different from the pre-movement baseline.

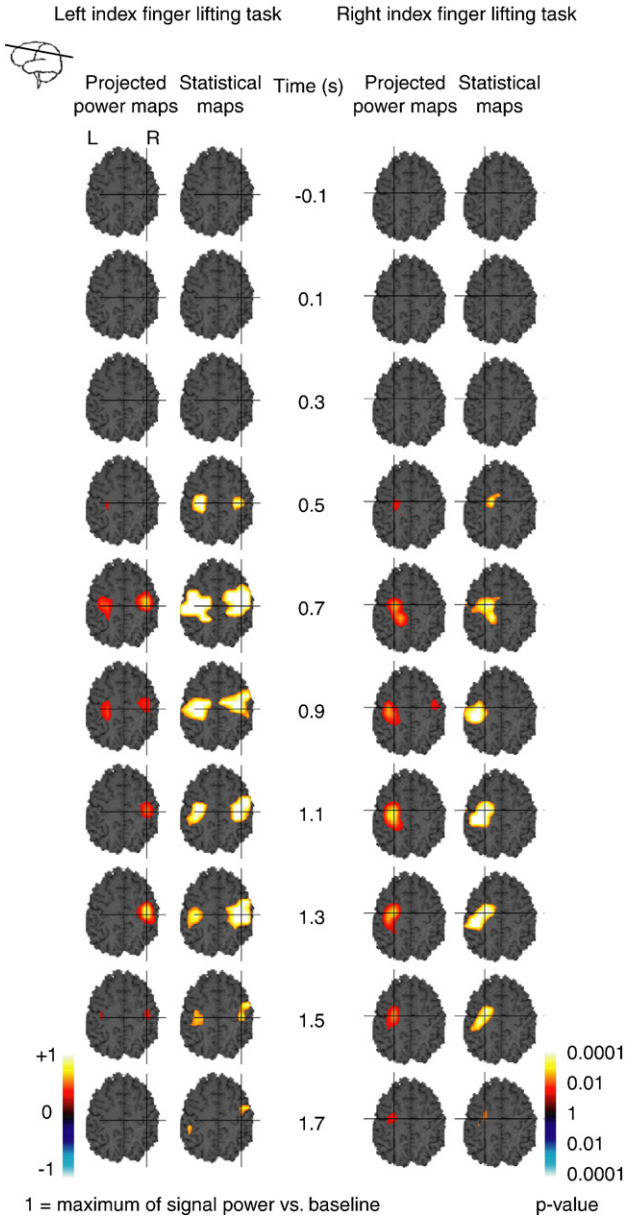

Fig. 6. Activity maps for right and left index finger lifting tasks. Both projected power and statistical maps are shown. The crosshair marks the location of maximum power for each case. Power maps indicate increased activity roughly from 0.5 s to 1.7 s, and the statistical maps demonstrate that the observed activity was statistically significant. The 20-Hz modulation appears more bilateral for left than right index finger movement. The baseline interval was set at −67 to 0 ms.

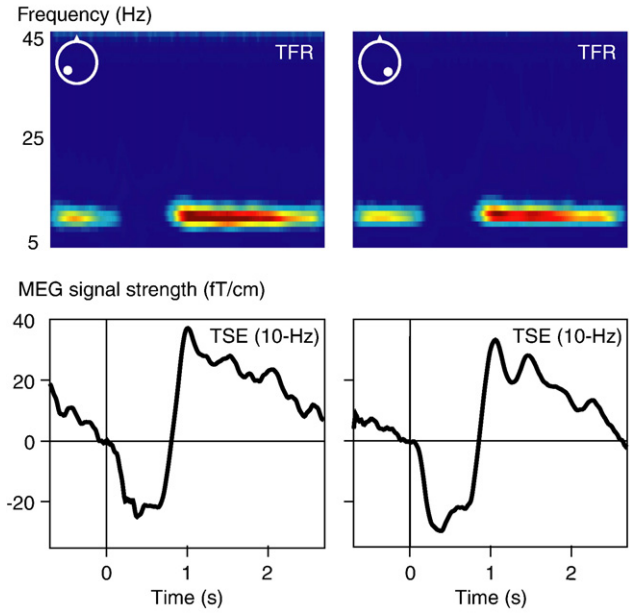

Fig. 7. Selection of frequency ranges and time windows in the word reading task. TFR plots and TSE curves for selected single sensors over the left and right occipitotemporal cortex (see schematic heads in the TFR plots). Rhythmic activity in the 10-Hz band (7–14 Hz) was strongly modulated over both hemispheres. The strongest suppression of rhythmic activity occurred at around 0.4 s and the maximum increase at around 1 s after word onset.

Based on the areas of activity indicated by the projected power and statistical maps, the left and right motor cortices were identified as source areas and introduced in a multidipole model. The two sources accounted well for the modulation of rhythmic activity, with a goodness-of-fit of 71% for the right and 79% for the left index finger movement.

Silent word reading task

This task was cognitively more demanding than the simple motor task described above. TFR plots on selected left and right occipito-temporal sensors that typically reflect reading-relevant activation (Salmelin, 2007) indicated 7–14 Hz as the frequency range of interest (Fig. 7). The TSE curves for this frequency range (cf. Fig. 9) implied that there were several active areas, but the main effects were observed in sensors located over the occipital and parietal areas, with maximum suppression at around 0.4 s and strong rebound at around 1 s (Fig. 7).

Based on the projected power and statistical maps (Fig. 8) two salient active areas were identified, one in the right occipital cortex, close to the midline, and the other more laterally in the left occipital cortex (sources 1 and 2 in Fig. 9). These areas showed the early suppression and later rebound of rhythmic activity that had been observed in the sensor-level TSE curves (Fig. 7). The statistical maps suggested presence of two additional source areas (sources 3 and 4 in Fig. 9). Together, the four localized areas were

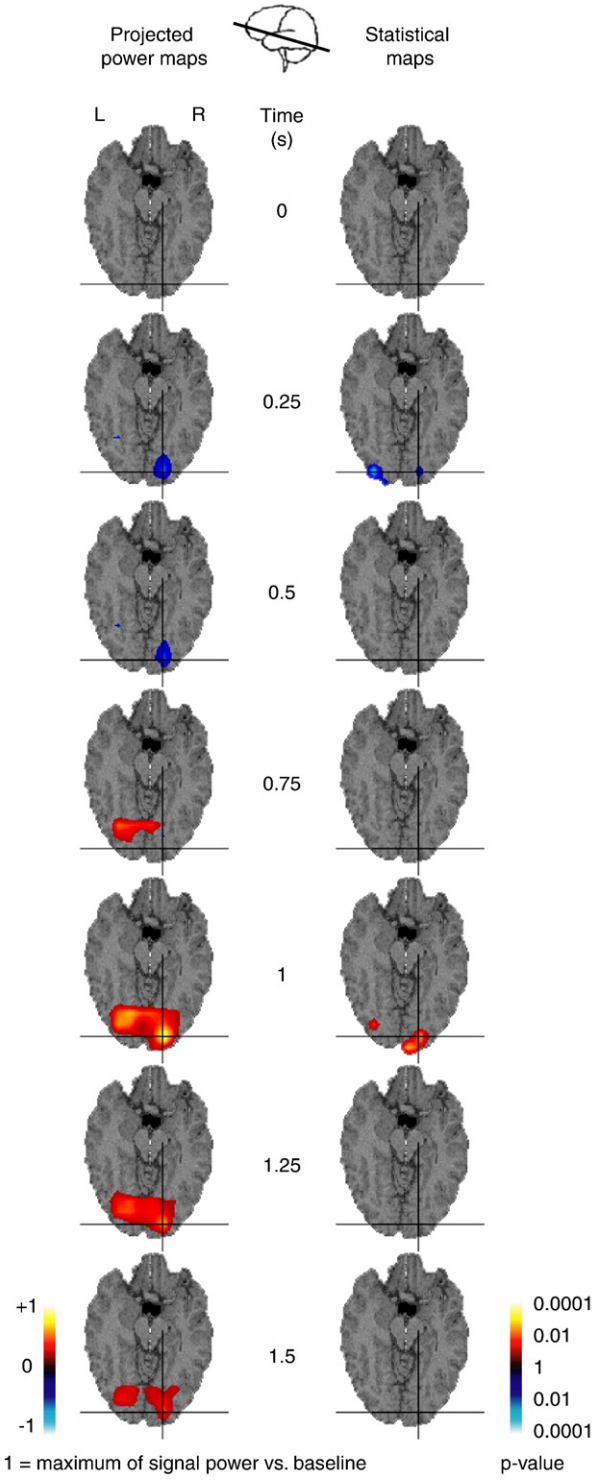

Fig. 8. Projected power and statistical maps in the word reading task. The displayed set of slices focuses on the occipital cortex. Suppression at around 0.4 s was followed by a strong bilateral rebound of 10-Hz activity at around 1 s. The baseline interval was set at −67 to 0 ms.

introduced in a multidipole model. This model accounted for most of the observed rhythmic activity (Fig. 9), with a goodness-of-fit of 79%.

Discussion

In this study, we introduced erDICS, an event-related version of Dynamic Imaging of Coherent Sources (Gross et al., 2001) that allows spatial mapping of the power level of oscillatory neural activity as a function of time, with respect to stimulus presentation or task performance. This approach thus complements evoked response analysis which is commonly used on neurophysiological

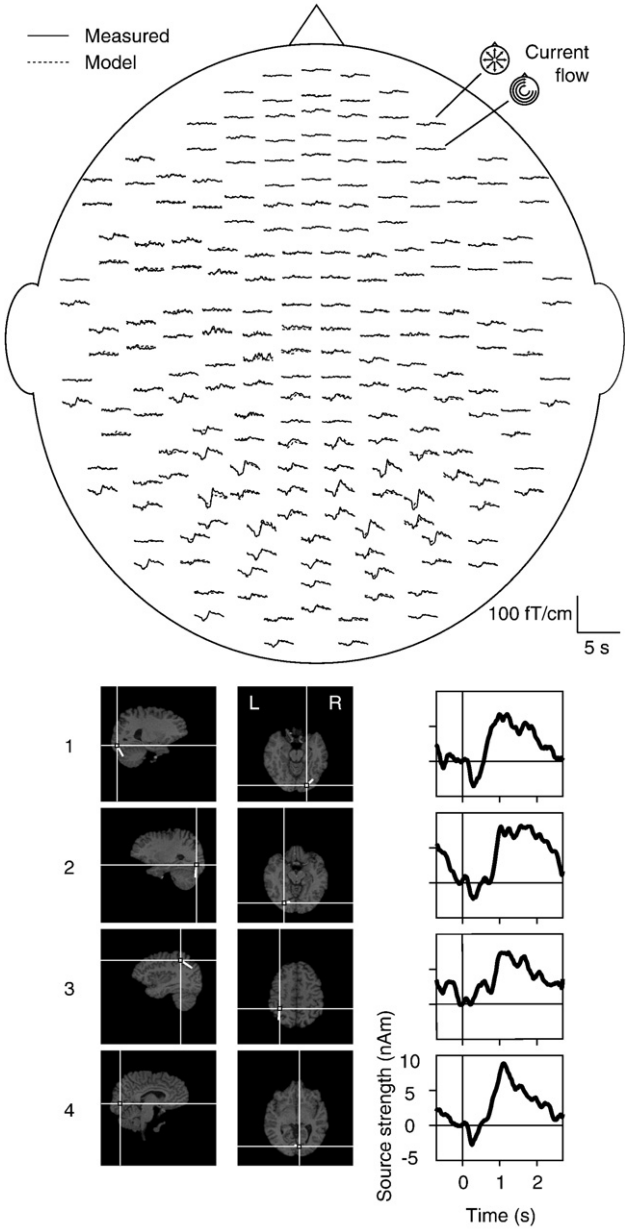

Fig. 9. Verification of the source analysis. Top: Original TSE (solid line) and TSE of the multidipole model (dashed line) for the silent reading task. The model explained the data well with a goodness-of-fit of 79% over all sensors and the whole analysis interval. At each recording site, there are two orthogonally oriented planar gradiometers (schematic heads in the upper right corner denote their sensitivity to direction of current flow). Bottom: Locations of the four ECDs included in the multidipole model and their source-level TSE waveforms.

(EEG, MEG) data to reveal changes of activity that occur systematically at the same time from trial to trial. Such analysis typically dismisses equally consistent event-related modulation of rhythmic activity because it is mostly not phase-locked to the stimulus or task timing. With the help of a time-resolved frequency-domain beamformer, erDICS yields the spatial distribution of both power suppressions and power increases in a chosen frequency range, at a chosen time, with respect to the power level during the pre-stimulus/task baseline interval. Permutation tests further reveal the areas in which the modulations of oscillatory power are statistically significant, in individual subjects. Importantly, the goodness of the results can be quantified by investigating how well the identified source areas explain the original measured data.

Simulations showed that erDICS performs well with reasonable noise levels typically encountered in real data. All the simulated cortical sources were identified down to SNR of 1/15, and about half of the sources (mostly during the rebound phase) even at the lowest SNR tested (1/20). The localization of the simulated sources was correct, within computational accuracy. At very low SNR the source areas spread out in space, reflecting the increasing uncertainty in localization of the sources. For a real MEG data set acquired during simple index finger lifting task, the rhythmic activity was readily localized in time and space, and it was centered on the hand motor cortex, bilaterally. Furthermore, on a more complex data set collected during a reading task a multidipole model based on regions identified with erDICS accounted for the modulation of rhythmic activity observed on the MEG sensors, thus confirming that the source areas and their time courses of activation correctly described the measured data.

In the analysis examples presented here, we used a CSD averaged across the whole data set, which turned out to be an efficient representation of the spectral and spatial relationships between sensors and, with the help of the frequency-domain beamformer, between brain areas. Intuitively, it would seem straightforward to use single-trial CSDs to reach to the brain level and perform further analysis on the resulting single-trial power maps. We tested this approach, but the combination of poor SNR in single-trial CSDs and unavoidable temporal spreading of wavelets resulted in blurring of modulation effects when they occurred fairly closely spaced in time. Furthermore, the averaged power maps were overall more spread out (reflecting increased uncertainty) than the maps projected to the brain with the help of an averaged CSD. Considerable increase in SNR would probably improve the accuracy of the single-trial CSD approach, in line with recent observations of the impact of experimental design and the amount of available data on the estimation of the covariance matrix used in SAM (Brookes et al., 2008). In real experiments, the adverse effect of low SNR on single-trial CSD estimate is, unfortunately, hard to overcome as the SNR of a single trial cannot usually be hugely increased, and the improvement of SNR would have to come from an increase in the number of trials. In experiments that use multiple conditions, or complex cognitive tasks, it is nearly impossible to acquire hundreds of trials per condition. With the SNRs tested here, mean CSD performed better than single-trial CSD approach in separating neural effects that were close in time.

Here we did not employ the full potential of a time-dependent CSD matrix, but used a time-averaged CSD which enhances the stability of the spatial filter. Averaging CSD over the whole time range of interest builds on the assumption that the source orientation does not change during the task. Obviously, this is the assumption usually made in the analysis of evoked responses, and has been successfully used in the field of MEG/EEG studies. This assumption could be incorrect if a voxel contains multiple sources of rhythmic activity that are active at different times and have different orientations. Further work will be needed to assess the advantages and pitfalls of using time-variant CSD for creating time-variant spatial filters. Most likely, a short moving-average time window will need to be used, and the effect of decreased SNR on the CSD estimate must be evaluated. The time-variant CSDs would have an obvious, significant application in the study of interareal coherence that the DICS method was originally developed for (Gross et al., 2001; Gross et al., 2002; Kujala et al., 2007). It is likely to become a major future application of erDICS. Nevertheless, event-related approximation of CSD matrix only utilizes parts of the measured data, as opposed to the entire data set in the original DICS method. It is as yet unclear how the limited SNR will affect the estimation of interareal coherence.

Statistical testing was implemented in order to improve the reliability of the results. We chose permutation test as it does not assume normality in the data and can easily be extended to handle the multiple comparisons problem via a maximum-statistics approach (Holmes et al., 1996; Nichols and Holmes, 2002). Permutation test is a technique commonly used in functional imaging studies with PET and fMRI, but it has recently been applied in MEG studies as well with the increased interest in spatial mapping (Pantazis et al., 2005; Singh et al., 2003). We developed and tested statistical analysis for the single-subject level in order to retain the possibility to evaluate each subject separately, which is the typical approach in MEG analysis. Here we used power and statistical maps in parallel, but a more automatic approach would be to use statistical maps as "masks" for power maps, i.e., one could employ the statistical maps for thresholding, or use the p-values as weights for the power maps. Group analysis can be readily implemented in various ways. One solution is to use the permutation test at the group level, as the problems are largely the same as those encountered at the individual level (non-normal distributions, multiple comparisons problem). The group-level approach has been used with SAM analysis (Chau et al., 2002; Singh et al., 2003).

A typical neuroscience experiment contains multiple experimental conditions, and one seeks to identify active areas, their time courses of activation, and any systematic variation in activation strength or timing between conditions. Here, we illustrated an approach where statistically significant event-related suppression and/or increase of rhythmic activity was taken to indicate neural activation, and the active areas were localized by comparing "active" time intervals to the pre-stimulus baseline interval. Let us assume that we would have an experiment with a parametric design, including two conditions A and B. We could localize the active areas in this same way separately for each condition. If the areas are approximately the same, we could model them as ECDs, check that they account for the measured data, and compare the time courses of activation in those brain areas between the experimental conditions. This approach is conceptually identical to typical analysis of evoked responses. Alternatively, one could directly compute power and statistical maps for a comparison between conditions A and B, at specific times. This approach would be more similar to that typically used in fMRI analysis, and it has been recently employed in SAM analysis of MEG data (McNab et al., 2007). In the erDICS method, the "active" vs. baseline comparison illustrated in the present report can easily be extended to a comparison between experimental conditions.

The power maps of rhythmic activity, and the corresponding statistical maps in individual subjects, lend themselves for direct

comparison with simultaneously recorded phase-locked evoked responses. Importantly, if one records both neurophysiological (MEG) and hemodynamic (fMRI) data on the same subjects, using a comparable experimental design in both modalities, these tools should make it possible to evaluate whether event-related modulations of rhythmic activity or traditional evoked responses correspond better with the fMRI activation maps. Such comparisons could provide important information not only on the relationship between imaging modalities but also on the nature of neural processing.

References

Brookes, M.J., Gibson, A.M., Hall, S.D., Furlong, P.L., Barnes, G.R., Hillebrand, A., Singh, K.D., Holliday, I.E., Francis, S.T., Morris, P.G., 2005. GLM-beamformer method demonstrates stationary field, alpha ERD and gamma ERS co-localisation with fMRI BOLD response in visual cortex. Neuroimage 26, 302–308.

Brookes, M.J., Vrba, J., Robinson, S.E., Stevenson, C.M., Peters, A.M., Barnes, G.R., Hillebrand, A., Morris, P.G., 2008. Optimising experimental design for MEG beamformer imaging. Neuroimage 39, 1788–1802.

Chatrian, G.E., Petersen, M.C., Lazarte, J.A., 1959. The blocking of the Rolandic wicket rhythm and some central changes related to movement. Electroencephalogr. Clin. Neurophysiol., Suppl. 11, 497–510.

Chau, W., Ishii, R., Ross, B., McIntosh, A.R., Pantev, C., 2002. Group analysis for the synthetic aperture magnetometry (SAM) data. In: Nowak, H., Haueisen, J., Giessler, F., Hounker, R. (Eds.), Proceedings of the 13th International Conference on Biomagnetism, pp. 1009–1011.

Cheyne, D., Barnes, G.R., Holliday, I.E., Furlong, P.L., 2000. Localization of brain activity associated with non-time-locked tactile stimulation using synthetic aperture magnetometry (SAM). In: Nenonen, J., Ilmoniemi, R.J., Katila, T. (Eds.), Proceedings of the 12th International Conference on Biomagnetism. Espoo, Finland, pp. 255–258.

Cheyne, D., Bakhtazad, L., Gaetz, W., 2006. Spatiotemporal mapping of cortical activity accompanying voluntary movements using an event-related beamforming approach. Hum. Brain Mapp. 27, 213–229.

Dale, A.M., Liu, A.K., Fischl, B.R., Buckner, R.L., Belliveau, J.W., Lewine, J.D., Halgren, E., 2000. Dynamic statistical parametric mapping: combining fMRI and MEG for high-resolution imaging of cortical activity. Neuron 26, 55–67.

Foucher, J.R., Otzenberger, H., Gounot, D., 2003. The BOLD response and the gamma oscillations respond differently than evoked potentials: an interleaved EEG-fMRI study. BMC Neurosci. 4, 22.

Furlong, P.L., Hobson, A.R., Aziz, Q., Barnes, G.R., Singh, K.D., Hillebrand, A., Thompson, D.G., Hamdy, S., 2004. Dissociating the spatiotemporal characteristics of cortical neuronal activity associated with human volitional swallowing in the healthy adult brain. Neuroimage 22, 1447–1455.

Gaetz, W., Cheyne, D., 2006. Localization of sensorimotor cortical rhythms induced by tactile stimulation using spatially filtered MEG. Neuroimage 30, 899–908.

Gross, J., Kujala, J., Hämäläinen, M., Timmermann, L., Schnitzler, A., Salmelin, R., 2001. Dynamic imaging of coherent sources: studying neural interactions in the human brain. Proc. Natl. Acad. Sci. U. S. A. 98, 694–699.

Gross, J., Timmermann, J., Kujala, J., Dirks, M., Schmitz, F., Salmelin, R., Schnitzler, A., 2002. The neural basis of intermittent motor control in humans. Proc. Nat. Acad. Sci. U. S. A. 99, 2299–2302.

Holmes, A.P., Blair, R.C., Watson, J.D., Ford, I., 1996. Nonparametric analysis of statistic images from functional mapping experiments. J. Cereb. Blood Flow Metab. 16, 7–22.

Hämäläinen, M.S., Sarvas, J., 1989. Realistic conductivity geometry model of the human head for interpretation of neuromagnetic data. IEEE Trans. Biomed. Eng. 36, 165–171.

Hämäläinen, M., Hari, R., Ilmoniemi, R.J., Knuutila, J., Lounasmaa, O.V., 1993. Magnetoencephalography — theory, instrumentation, and applications to noninvasive studies of the working human brain. Rev. Mod. Phys. 65, 413–497.

Jensen, O., Gelfand, J., Kounios, J., Lisman, J.E., 2002. Oscillations in the alpha band (9–12 Hz) increase with memory load during retention in a short-term memory task. Cereb. Cortex 12, 877–882.

Jensen, O., Vanni, S., 2002. A new method to identify multiple sources of oscillatory activity from magnetoencephalographic data. Neuroimage 15, 568–574.

Kujala, J., Pammer, K., Cornelissen, P., Roebroeck, A., Formisano, E., Salmelin, R., 2007. Phase coupling in a cerebro-cerebellar network at 8–13 Hz during reading. Cereb. Cortex 17, 1476–1485.

Liljeström, M., Kujala, J., Jensen, O., Salmelin, R., 2005. Neuromagnetic localization of rhythmic activity in the human brain: a comparison of three methods. Neuroimage 25, 734–745.

Lin, F.H., Witzel, T., Hämäläinen, M.S., Dale, A.M., Belliveau, J.W., Stufflebeam, S.M., 2004. Spectral spatiotemporal imaging of cortical oscillations and interactions in the human brain. Neuroimage 23, 582–595.

Lounasmaa, O.V., Hämäläinen, M., Hari, R., Salmelin, R., 1996. Information processing in the human brain: magnetoencephalographic approach. Proc. Natl. Acad. Sci, U. S. A. 93, 8809–8815.

Maris, E., Oostenveld, R., 2007. Nonparametric statistical testing of EEG- and MEG-data. J. Neurosci. Methods 164, 177–190.

McNab, F., Rippon, G., Hillebrand, A., Singh, K.D., Swithenby, S.J., 2007. Semantic and phonological task-set priming and stimulus processing investigated using magnetoencephalography (MEG). Neuropsychologia 45, 1041–1054.

Nichols, T.E., Holmes, A.P., 2002. Nonparametric permutation tests for functional neuroimaging: a primer with examples. Hum. Brain Mapp. 15, 1–25.

Niessing, J., Ebisch, B., Schmidt, K.E., Niessing, M., Singer, W., Galuske, R.A., 2005. Hemodynamic signals correlate tightly with synchronized gamma oscillations. Science 309, 948–951.

Pammer, K., Hansen, P.C., Kringelbach, M.L., Holliday, I., Barnes, G., Hillebrand, A., Singh, K.D., Cornelissen, P.L., 2004. Visual word recognition: the first half second. Neuroimage 22, 1819–1825.

Pammer, K., Hansen, P., Holliday, I., Cornelissen, P., 2006. Attentional shifting and the role of the dorsal pathway in visual word recognition. Neuropsychologia 44, 2926–2936.

Pantazis, D., Nichols, T.E., Baillet, S., Leahy, R.M., 2005. A comparison of random field theory and permutation methods for the statistical analysis of MEG data. Neuroimage 25, 383–394.

Pfurtscheller, G., 1992. Event-related synchronization (ERS): an electrophysiological correlate of cortical areas at rest. Electroencephalogr. Clin. Neurophysiol. 83, 62–69.

Pfurtscheller, G., Aranibar, A., 1979. Evaluation of event-related desynchronization (ERD) preceding and following voluntary self-paced movement. Electroencephalogr. Clin. Neurophysiol. 46, 138–146.

Pfurtscheller, G., Lopes da Silva, F.H., 1999. Event-related EEG/MEG synchronization and desynchronization: basic principles. Clin. Neurophysiol. 110, 1842–1857.

Robinson, S.E., Vrba, J., 1997. Functional neuroimaging by Synthetic Aperture Magnetometry (SAM). In: Yoshimoto, T., Kotani, M., Kuriki, S., Karibe, H., Nakasato, B. (Eds.), Recent Advances in Biomagnetism. Tohoku University Press, Sendai, pp. 302–305.

Saarinen, T., Laaksonen, H., Parviainen, T., Salmelin, R., 2006. Motor cortex dynamics in visuomotor production of speech and non-speech mouth movements. Cereb. Cortex. 16, 212–222.

Salmelin, R., 2007. Clinical neurophysiology of language: the MEG approach. Clin. Neurophysiol. 118, 237–254.

Salmelin, R., Hari, R., 1994. Spatiotemporal characteristics of sensorimotor neuromagnetic rhythms related to thumb movement. Neuroscience 60, 537–550.

Salmelin, R., Sams, M., 2002. Motor cortex involvement during verbal versus non-verbal lip and tongue movements. Hum. Brain Mapp. 16, 81–91.

Salmelin, R., Hämäläinen, M., Kajola, M., Hari, R., 1995. Functional segregation of movement-related rhythmic activity in the human brain. Neuroimage 2, 237–243.

Salmelin, R., Schnitzler, A., Schmitz, F., Freund, H.J., 2000. Single word reading in developmental stutterers and fluent speakers. Brain 123, 1184–1202.

Sekihara, K., Nagarajan, S.S., Poeppel, D., Marantz, A., 2004. Performance of an MEG adaptive-beamformer source reconstruction technique in the presence of additive low-rank interference. IEEE Trans. Biomed. Eng. 51, 90–99.

Singer, W., 1999. Neuronal synchrony: a versatile code for the definition of relations? Neuron 24, 49–65.

Singh, K.D., Barnes, G.R., Hillebrand, A., Forde, E.M., Williams, A.L., 2002. Task-related changes in cortical synchronization are spatially coincident with the hemodynamic response. Neuroimage 16, 103–114.

Singh, K.D., Barnes, G.R., Hillebrand, A., 2003. Group imaging of task-related changes in cortical synchronisation using nonparametric permutation testing. Neuroimage 19, 1589–1601.

Steriade, M., Gloor, P., Llinás, R.R., Lopes da Silva, F.H., Mesulam, M.-M., 1990. Basic mechanisms of cerebral rhythmic activities. Electroenceph. Clin. Neurophysiol. 76, 481–508.

Tallon-Baudry, C., Bertrand, O., Delpuech, C., Permier, J., 1997. Oscillatory gamma-band (30–70 Hz) activity induced by a visual search task in humans. J. Neurosci. 17, 722–734.

Van Veen, B.D., Buckley, K., 1988. Beamforming: a versatile approach to spatial filtering. IEEE ASSP Mag. 5, 4–24.

Van Veen, B.D., van Drongelen, W., Yuchtman, M., Suzuki, A., 1997. Localization of brain electrical activity via linearly constrained minimum variance spatial filtering. IEEE Trans. Biomed. Eng. 44, 867–880.

Wydell, T.N., Vuorinen, T., Helenius, P., Salmelin, R., 2003. Neural correlates of letter-string length and lexicality during reading in a regular orthography. J. Cogn. Neurosci. 15, 1052–1062.